Magnetoresistance properties of thin films of the metallic oxide ferromagnet $SrRuO_3$

S. C. Gausepohl and Mark Lee
Department of Physics, University of Virginia, Charlottesville, Virginia 22903

K. Char
Conductus, Inc., 969 West Maude Avenue, Sunnyvale, California 94086

R. A. Rao and C. B. Eom
Department of Mechanical Engineering and Materials Science, Duke University, Durham, North Carolina 27708
(Received 27 December 1994; revised manuscript received 14 April 1995)

The magnetoresistance of epitaxial thin films (250 to 1000 Å thick) of the metallic oxide ferromagnet $SrRuO_3$ has been measured at temperatures ranging from well below to just above the Curie point (≈ 160 K). Measurements using both transverse (nonzero Lorentz force) and longitudinal (zero Lorentz force) geometries cleanly distinguish between an orbital contribution, present only at low temperature, and a spin-flip scattering contribution, present at all temperatures, to the resistivity in magnetic field. The magnetoresistance also shows strongly hysteretic behavior with high coercive and saturation fields. Through the Curie point, the magnetoresistance magnitude shows a maximum, which results from the suppression of the phase transition in magnetic field. The temperature derivative of the zero-field resistivity also shows a discontinuous jump, as predicted by standard theory.

I. INTRODUCTION

As a consequence of intensive research on the oxide high-temperature superconductor materials, there has been a revival of interest in oxide normal (nonsuperconducting) metals as well. This interest has been stimulated by the search for lattice-matched, nonreactive metals for use in the development of proximity-coupled Josephson junctions. This search has also led to the realization that the metallic oxides possess a large array of interesting physical phenomena in their own right, ranging from strong Coulomb interactions to ferromagnetism to optical transparency, many of which are not fully understood. Charge transport in the metallic oxides differs qualitatively from conventional metals. The room-temperature resistivity of nearly all metallic oxides is ~ 100 $\mu\Omega$ cm, about 100 times larger than conventional metals. Electrical conduction in metallic oxides depends strongly on the hybridization between the cation constituents and oxygen.

In this paper we report detailed magnetoresistance measurements on thin films of the ferromagnetic oxide metal $SrRuO_3$. This material is one of very few oxide metals that shows ferromagnetic order as opposed to the more common antiferromagnetism seen in many oxide metals and semiconductors. At the present time it is not understood why $SrRuO_3$ is ferromagnetic, while many closely related ruthenates, such as $CaRuO_3$, are not.[1] It is possible that ferromagnetism in $SrRuO_3$ arises from an itinerant polarized conduction band. Therefore characterizing the interplay between the band-structure conduction and the ferromagnetism is important to understanding the nature of magnetic order in $SrRuO_3$.

The organization of the paper is as follows. Section II discusses $SrRuO_3$ and reviews relevant aspects of magnetoresistance theory. Section III discusses the experiment and data. Section IV offers an analysis of the data within standard magnetoresistance theory. Section V summarizes.

II. BACKGROUND

A. Properties of the $SrRuO_3$

$SrRuO_3$ was synthesized in 1959 by Randall and Ward[2] as part of a larger study of ruthenate compounds. The crystal structure was found to be orthorhombic with lattice constants $a^O=5.56$ Å, $b^O=5.53$ Å, and $c^O=7.84$ Å. It has a subunit cell that is a pseudocubic perovskite with lattice constants $a^P=b^P=c^P=3.93$ Å. For the purposes of this paper, the Miller indices for $SrRuO_3$ will be given with respect to the perovskite cell,[3] denoted by a superscript P.

In the 1960s and 1970s, Callaghan, Moeller, and Ward,[4] Longo, Raccah, and Goodenough,[5] and Kanbayashi[6] investigated several basic magnetic and electronic properties of single-crystal $SrRuO_3$ samples. They found it to be a metal ($\rho \approx 300$ $\mu\Omega$ cm at 300 K) with a ferromagnetic phase transition at a Curie temperature (T_c) of ~ 160 K. These authors also suggested that the ferromagnetism arises from an itinerant electron band rather than localized moments. Several characteristic magnetic values were measured during this period. The saturation moments reported are between 0.85 and 2.5 Bohr magnetons per Ru atom. In single crystals, large values of the coercive force (≈ 3 kG) and the remanence (≈ 14 emu/g) were also found.

Other than some neutron-diffraction experiments[7] on $SrRuO_3$ powder specimens to more accurately determine the magnetic and lattice properties, little work on the

0163-1829/95/52(5)/3459(7)/$06.00

perovskite ruthenates was done until 1991. Spurred on by interest in the high-temperature cuprate superconductors, there has been vigorous renewed interest in thin films of nonsuperconducting oxide metals in general and $SrRuO_3$ in particular. Since the lattice constants of the pseudoperovskite unit cell of $SrRuO_3$ are nearly equal to the a and b lattice constants of the high-T_c superconductor $YBa_2Cu_3O_7$, it is in principle possible to grow epitaxial thin-film superconductor–normal-metal (S-N) structures for Josephson device work. Initial work on ruthenate thin-film synthesis was pursued by Eom *et al.*[8] and Antognazza *et al.*,[9] leading to successful synthesis of epitaxial $SrRuO_3$ on a variety of substrates. Detailed structural and magnetic phase transition studies of $SrRuO_3$ films were recently reported by Catchen, Rearick and Schlom.[1] These works directly led to the growth of $YBa_2Cu_3O_7$ on $SrRuO_3$ thin films and the successful fabrication of Josephson junctions coupling two layers of $YBa_2Cu_2O_7$ through an intervening $SrRuO_3$ normal-metal weak link.[9–11] It was noted in Ref. 9 that the observed Josephson effect is inconsistent with the conventional understanding of superconductivity, since ferromagnetism and BCS superconductivity cannot coexist. It is presently unknown whether this unusual phenomenon is a peculiarity of transport in $SrRuO_3$ thin films grown on $YBa_2Cu_3O_7$, or of the superconductivity in $YBa_2Cu_3O_7$. In order to clarify this issue, a better understanding of charge transport in $SrRuO_3$ thin films is required.

B. Magnetoresistance

In this paper, we define magnetoresistance (MR) as the change in resistivity $[\Delta\rho=\rho(H)-\rho(0)]$, normalized to the zero-field resistivity $\rho(0)$, upon application of an external magnetic field H. There are many different classical and quantum origins of magnetoresistance in metals. The relevant mechanisms are reviewed here.

A change in resistance arising from Lorentz force perturbations of real- or reciprocal-space charge trajectories is defined as an "orbital" MR. The simplest case is an isotropic material in a "weak" (as defined below) magnetic field **H** perpendicular to the current density **J**, termed the transverse geometry. In zero field the current distributes itself to find the paths of least resistance. In a transverse field, the real-space charge trajectories are bent away from their zero-field paths by the Lorentz force, proportional to $\mathbf{J}\times\mathbf{H}$. Since the new paths are no longer necessarily the paths of least resistance, the effective mean free path (l) and scattering lifetime (τ) will decrease. To estimate this correction to the resistivity, i.e., the magnetoresistance, Abrikosov[12] suggested that the path difference can be found by subtracting the length of a chord from its corresponding arc of a circle. This gives a transverse MR $\Delta\rho/\rho(0)\approx(l/l_H)^2$, where l is the mean free path and $l_H=(cp_F/eH)$ is the Larmor radius of a charge with Fermi momentum p_F. This results in a positive quadratic dependence of the MR on H. Noting that $l\propto\tau$ and using the cyclotron frequency $\omega_c=(eH/m^*c)$, where m^* is the effective mass, the relationship can be written in the common form known as Kohler's rule: $\Delta\rho/\rho(0)\propto(\omega_c\tau)^2$ for the case of "weak" magnetic fields $\omega_c\tau<1$.

A larger transverse MR can occur if a system has multiple bands, giving rise to parallel current trajectories in reciprocal space. A standard calculation[13] shows that, if the bands are either all electronlike or all holelike, the MR again increases as $+H^2$ in weak field ($\omega_c\tau<1$), and saturates in strong fields ($\omega_c\tau>1$). The presence of multiple uncompensated bands generally yields a significantly larger-magnitude effect than a simple perturbation of real-space trajectories. In a compensated material, the MR continues to diverge as $+H^2$ in both weak and strong fields.

In a metal with magnetic spins, an additional quantum-mechanical scattering mechanism is possible. This is "spin-flip" or "spin-exchange" scattering, where a conduction electron scatters by exchanging spin with a magnetic moment or spin excitation. An external magnetic field increases the energy needed to flip a spin and thus decreases the amplitude for spin-flip scattering. All other effects being equal, the resistivity then decreases in a field, yielding a negative MR (i.e., $\Delta\rho<0$). A simple consideration of the weak-field spin-flip scattering amplitude between an electron and a single local magnetic moment is given by Abrikosov,[12] who derives $\Delta\rho/\rho(0)=-\alpha(\mu H)^2$, where α is a positive constant and μ is the moment per magnetic scatterer. The spin-flip scattering from exchange between conduction electrons and spin excitations in an itinerant ferromagnet was considered by Herring.[14] More sophisticated calculations of the field and temperature dependencies of spin-flip scattering between conduction electrons and various kinds of dynamic spin fluctuations were done by Mills and Lederer[15] and are reviewed by Moriya.[16] The general conclusion is that the spin exchange leads to a MR of *opposite sign* to the orbital case. Another crucial difference between the orbital and spin-flip mechanisms is that the spin-flip suppression is independent of the Lorentz force. It is present even if $\mathbf{J}\times\mathbf{H}=\mathbf{0}$, so the spin-flip and the orbital effects can be cleanly separated by measurements of both the transverse ($\mathbf{J}\perp\mathbf{H}$) and longitudinal ($\mathbf{J}\|\mathbf{H}$) MR's.

C. Ferromagnetic phase transition

A simple general description of magnetic properties through a second-order ferromagnetic phase transition can be found by applying mean-field theory.[17] The order parameter of the phase transition is the magnetization M, which grows just below T_c as $(T_c-T)^\beta$ where the mean-field exponent $\beta=\frac{1}{2}$. It can be shown that in a ferromagnet the derivative of the resistivity vs temperature, $d\rho/dT$, is proportional to the same spin-spin correlation function that determines the specific heat.[18] Since in mean-field theory the specific heat undergoes a discontinuous step increase through T_c,[19] this implies that $d\rho/dT$ should show a similar step discontinuity through T_c, so that $\rho(T)$ should show a break in slope at T_c. Therefore a jump in $d\rho/dT$ can be used in the same manner as the specific heat to identify a ferromagnetic phase transition.

D. Hysteresis

In a ferromagnet, the large numbers of magnetic moments can lower their macroscopic dipolar interaction energy through the formation of magnetic domains, between which the net alignment is either perpendicular or antiparallel.[20] In an external magnetic field, domains with preferential alignment tend to grow and invade neighboring counteraligned domains. Ideally, this domain-wall motion is reversible to the original zero-field domain structure. However, defects in real materials may act as pinning sites that must be overcome before a domain wall may pass. This makes the magnetic domain evolution irreversible and results in the hysteresis common to all real ferromagnets. In order to return to a zero-magnetization value, a finite reverse field, the coercive force, must be applied. Because the reversibility of the domain-wall motion is dependent on defect structure, hysteresis effects are normally strongly dependent on a sample's microstructure and hence are not truly intrinsic properties.

III. EXPERIMENT AND DATA

A. Experimental details

Thin-film samples of $SrRuO_3$ films were deposited by either laser ablation or single-target 90° off-axis sputtering[21,22] onto edge-oriented (100) single-crystal $LaAlO_3$ substrates. X-ray diffraction showed the $SrRuO_3$ films to be oriented with $[001]^P$ normal to the substrate, with in-plane twinning of the $[100]^P$ and $[010]^P$ axes. Samples ranged in thickness from 250 to 1000 Å. Using standard photolithographic techniques and etching with a 500 eV Ar^+ ion beam, we patterned four-point resistivity lines into each sample. The dimensions between the voltage leads were 2 mm × 100 μm (length × width). Ohmic electrical contact was achieved with silver epoxy attachment of copper wires to contact pads. Resistance was measured by biasing the sample with an ac current (500–1000 Hz) and detecting the resulting voltage drop by lock-in techniques. Bias amplitude was kept small enough to guarantee the response was Ohmic. The samples were mounted, one by one, on a Cu probe head that could be dropped into a cryostat chamber. A resistive heater and calibrated carbon-glass resistor mounted in the Cu probe head were used to control and measure temperature between 1.2 and 300 K. The resistivity as a function of temperature for a typical sample is shown in Fig. 1. A superconducting solenoid was used to apply magnetic field from 0 to 9 T.

The magnetoresistance of the $SrRuO_3$ films was examined in two different field geometries, which are defined here. Transverse perpendicular ($TMR_\perp$) denotes that the current direction is at right angles to the magnetic field H (i.e., transverse), and that the magnetic field is perpendicular to the plane of the film (i.e., $\perp$). The other configuration is longitudinal (LMR), which describes a field parallel to the current, and hence also to the plane of the film. For the LMR geometry, the field is parallel to either an in-plane [100] or [010] direction of the substrate, and therefore to the twinned $[100]^P$ and $[010]^P$

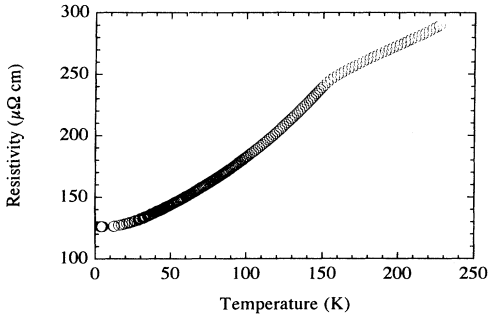

FIG. 1. Temperature dependence of the resistivity for a 250-Å-thick $SrRuO_3$ film.

directions of the $SrRuO_3$ films. Positive magnetoresistance is defined as an increase of the resistivity in magnetic field, compared to the zero-field value. Negative magnetoresistance indicates a decrease of the resistivity in field.

B. Data

The data fall into three areas of interest. The first concerns the similarities and differences of the MR curve shapes in the two geometries, which are intrinsic properties of the material. The second deals with hysteretic effects found in the MR curves, which are a consequence of the magnetic domain structure. Lastly, we describe the behavior of the magnetoresistance near the Curie point ($T_c = 158 \pm 2$ K). Data shown are representative of all samples.

MR curve shapes. The $TMR_\perp$ curves as a function of applied magnetic field at two temperatures well below the Curie point for a 900-Å-thick $SrRuO_3$ film are shown in Fig. 2. These data were taken by first cooling the sample to 5.2 K in zero magnetic field, taking a MR trace at this temperature by ramping the field up and down, then increasing the temperature up to 20.5 K. The low-field behavior of the initial ramp up in field at 5.2 K is qualitatively different from all subsequent field sweeps. The ini-

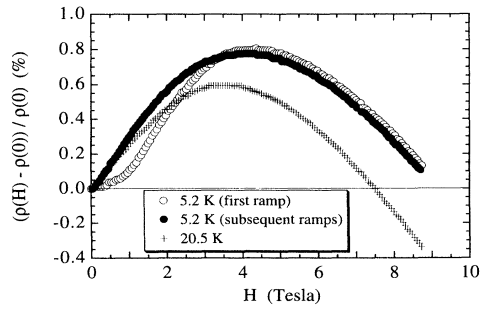

FIG. 2. Transverse magnetoresistance curves at 5.2 and 20.5 K for a 900-Å-thick $SrRuO_3$ film. The sample was cooled to 5.2 K in zero field. Open circles mark the first field ramp up to 9 T at 5.2 K. Dark circles indicate all subsequent field ramps up or down at 5.2 K. Temperature was then increased to 20.5 K.

tial ramp up produced a $TMR_{\perp}$ curve that is positive and parabolic ($\propto +H^2$) for $H \leq 2$ T, but the return (down) ramp data break away from the sweep up data and become a linear function as $H \rightarrow 0$. After the initial ramp up, there is no difference between data taken ramping the field up or down at any fixed temperature, as long as the sample is maintained below T_c. Up to ~70 K, the $TMR_{\perp}$ data are all positive and approximately linear at fields ≤ 1 T. Each trace shows a maximum, which decreases both in magnitude and field position with increasing temperature. For instance, the maximum at 5.2 K occurs around 4.2 T and peaks near +0.8%, while at 20.5 K it occurs around 3.8 T and peaks at +0.6%. The maxima are broad, and at the higher temperatures there is a crossover from positive to negative MR at higher field.

Figure 3 shows the effect of geometry on the low-temperature MR curves. Typically, each field sweep consisted of roughly 100 data points, of which only a few are marked for clarity. All data in this figure were taken near 10 K on one 250 Å sample, but in different geometries. The circles and triangles indicate the $TMR_{\perp}$ and LMR geometries respectively. The geometry was changed between measurements by bringing the sample out of the cryostat to room temperature, rotating the sample, then cooling back down in zero field. Black symbols mean the data were taken during the initial field ramp up in each case, while the white symbols are for all subsequent field sweeps up or down at this temperature. In both geometries, the initial ramp up and all later field sweeps do not overlap below 4 T. The $TMR_{\perp}$ geometry data show positive MR with a broad maximum consistent with Fig. 2. The entire LMR curve has negative MR values, with a large magnitude change from zero field (about −5% near 7 T). The magnitude of the LMR data also increases quadratically at lower fields on the initial ramp up, and returns back in a quasi-linear fashion upon decreasing the field back to zero.

The inset of Fig. 3 shows the MR behavior at 150 K (just below the Curie point), using the same sample as in the main figure. In each geometry, these data were recorded following the data of the main figure, after raising the temperature to 150 K. Up and down field sweeps are equivalent in each geometry since the initial ramp up was done at 10 K. At 150 K, both orientations show negative MR; that is, the positive contribution to the TMR at low temperature disappears at higher temperature. In fact, we observed the TMR to become negative at all fields for temperatures above 70 K. This higher-temperature negative MR has a roughly linear dependence of H in both orientations.

Hysteresis. A strong MR hysteresis curve, symmetric around zero field, is shown in Fig. 4(a). These data correspond to a 250-Å-thick sample in the $TMR_{\perp}$ geometry, held at 1.19 K. The sample was cooled in zero field and immersed in liquid He. Temperature was both monitored and controlled by maintaining the He partial pressure over the liquid. When 1.19 K was reached, the field was first ramped up and back, then the magnet leads were switched to reverse the polarity of the field. The initial sweep up, shown as + signs leading away from "START," approaches the main hysteresis curve in the same quadratic manner as shown in Fig. 2. The slope crossover is present in both polarities, each mirroring the other side. The bold arrows indicate the directions of the field sweeps. As the magnet changes polarity, the MR signal traces out a butterfly-shaped curve. The forward and back sweeps overlap around 3.5 T, which corresponds to the saturation field in the magnetization hysteresis [Fig. 4(b)]. The hysteresis itself is the result of an overshoot by the signal as it approaches and then passes zero field from both above and below. The minima in the

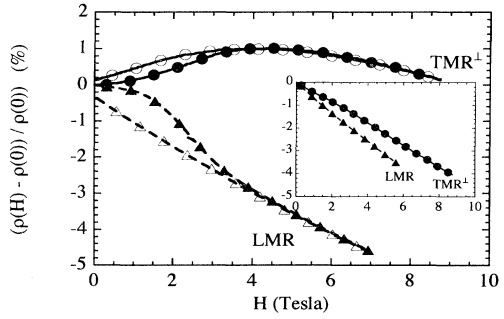

FIG. 3. Magnetoresistance in the TMR (circles) and LMR (triangles) geometries at 10 K. The sample was zero-field cooled. Dark symbols indicate initial field ramps, and the open symbols show all subsequent field ramps at that temperature. Inset: Magnetoresistance in the two geometries at 150 K. Axis units are the same as in the main figure. For both geometries, initial field ramps were done at 10 K before warming the sample to 150 K.

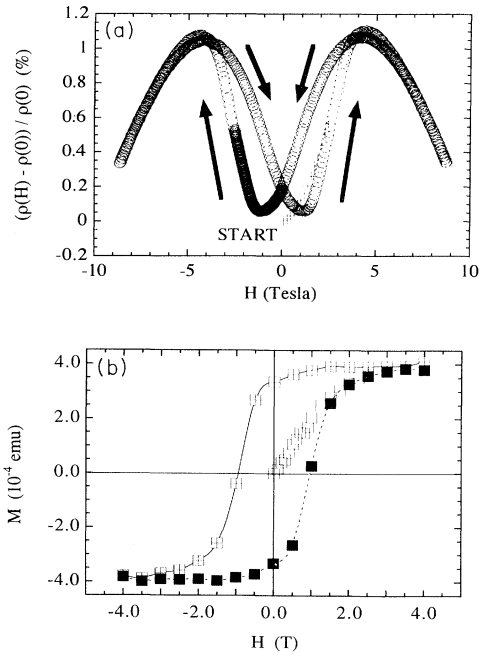

FIG. 4. (a) $TMR_{\perp}$ of a 250-Å-thick $SrRuO_3$ film, cooled in zero field, taken with both field polarities at 1.19 K. The + symbols indicate data taken on the first field ramp up. (b) Magnetoresistance hysteresis loop of a $SrRuO_3$ film as a function of applied field H at 4.2 K.

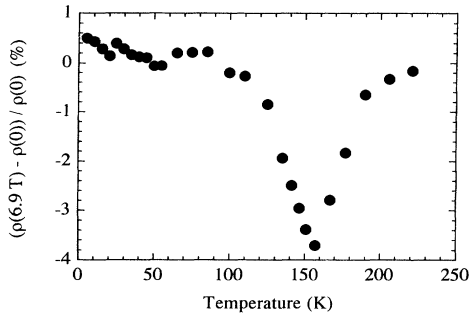

FIG. 5. The transverse magnetoresistance value in a field of 6.9 T taken at several temperatures through T_c. The sample was zero-field cooled to 5 K and the field was ramped up and down at each temperature.

$TMR_\perp$ data near ± 1 T, are still positive with respect to the initial $H=0$ resistivity, and correspond to the coercive field ($M=0$) in Fig. 4(b). After the initial ramp, the butterfly shape repeats itself as the magnet cycles through positive and negative field directions.

Critical behavior. The magnitude of the negative MR increases as T approaches T_c from both above and below, as can be seen clearly by the plot of the MR at $H=6.9$ T versus temperature shown in Fig. 5. Here a film in the $TMR_\perp$ geometry was cooled to 5 K in zero field. After stabilizing the temperature at each point shown, the MR was taken by ramping the field up to 8 T and back to 0 T. The temperature was then increased. The collected MR values at $H=6.9$ T for each run were graphed together. The result is a large negative dip (around -4%) at T_c.

The kink in the resistivity (Fig. 1) that appears at T_c in $H=0$ can be more closely examined through a first derivative. A digital derivative was taken and is shown in Fig. 6. At high temperatures, $d\rho/dT$ is relatively constant. At T_c it takes jumps up to a higher value, and falls roughly linearly as the temperature is lowered. Figure 6 also shows $d\rho/dT$ taken by cooling the sample in a field of 5.2 T. For these data, the sample was first warmed to ~ 280 K in zero field. Then the magnetic field was applied, the magnet was set to persistent current mode, and the sample was cooled. While $d\rho/dT$ is not constant in this temperature range, it is clearly seen that the jump at

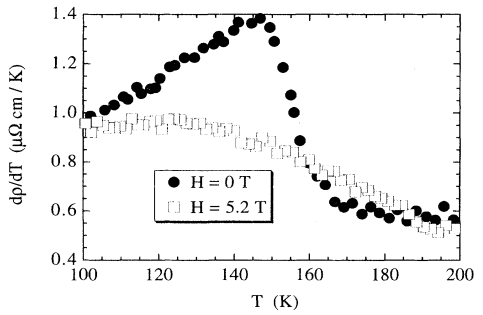

FIG. 6. First derivative of the resistivity with respect to temperature in zero field and in 5.2 T. The 5.2 T data were taken by cooling the sample from above T_c in fixed field.

T_c is greatly suppressed in a high magnetic field. Above ~ 5 T, the resistivity through the transition is smooth. The MR in both geometries is negative for $T > 70$ K; that is, the resistivity in 5 T is smaller than the zero-field value.

IV. DATA ANALYSIS

Magnetoresistance. The data clearly show two competing weak-field MR mechanisms in $SrRuO_3$ at low temperature. One process yields a positive MR, while the other results in a negative MR. In the low-temperature TMR data there is a crossover from dominant positive MR behavior at lower fields to dominant negative MR behavior at higher fields, resulting in the maximum evident in Fig. 2. The fact that the positive MR does not appear in the LMR data shows unequivocally that the positive effect is *dependent* upon the Lorentz force and is therefore, by definition, an orbital effect. The positive H^2 field dependence (on the initial magnetic field ramp) and the disappearance of the positive component of the TMR at higher temperature are both characteristic of orbital magnetoresistance in the weak-field limit. Conversely, the LMR data show that the negative MR is independent of the Lorentz force and is therefore most likely a purely spin-dependent effect that competes with the orbital effects in the TMR geometry.

Ascertaining the physical origin of the orbital MR is complicated because the data are all in the weak-field limit, due to strong scattering effects in the $SrRuO_3$ films. Our Hall effect measurements[23] on the (Ca,Sr)RuO_3 system give a carrier density of about 2×10^{22} cm^{-3}, not much smaller than that of conventional metals. Therefore the resistivity of ~ 100 $\mu\Omega$ cm at 4.2 K indicates a total scattering lifetime two to three orders of magnitude smaller than in conventional metals, so that $\omega_c\tau \ll 1$ at all achievable fields. From the resistivity and the carrier density, the mean free path l is estimated to be <200 Å at 4.2 K, compared to a Larmor radius $l_H \approx 2$ μm at $H=2$ T where the positive H^2 TMR is prominent. If we assume that the orbital MR arises solely from real-space path perturbations in the weak-field limit, these numbers yield a TMR magnitude

$$\Delta\rho(2\text{ T})/\rho(0) \approx (l/l_H)^2 \leq 0.01\% ,$$

which is ~ 100 times smaller than what is observed. This discrepancy provides strong evidence that the positive TMR does not result principally from perturbation of the real-space current trajectories.

The orbital MR is also not fully consistent with generic band-structure effects. A comparison of the functional shapes of the negative LMR and the TMR for $H > 4$ T at 5 K (Fig. 2) shows that the positive orbital contribution cannot continue to increase as $+H^2$ at higher field. The magnitude of the LMR data above 4 T (Fig. 3) increases slightly more slowly than $-H^{1.00}$, with a simple power-law fit giving a $-H^{0.92}$ dependence. Therefore, if the positive MR contribution continued to increase as $+H^2$, as predicted by all weak-field MR models, it would dominate the negative MR contribution through 9 T. The fact that the low-temperature TMR is positive at lower

fields but rapidly gives way to the negative MR as H increases past 4 T means that the orbital contribution to the TMR must increase more slowly than $+H$ above 4 T. This rules out large TMR effects from carrier compensation or open orbits, both of which increase as $+H^2$ in all field regimes. While a simple two-band MR model[13] does predict a diminishing resistance increase in the strong-field ($\omega_c\tau > 1$) limit, the large value of the resistivity keeps the samples well within the weak-field regime ($\omega_c\tau \ll 1$) up to the highest fields used. Therefore the inferred weakening of the positive TMR cannot be simply interpreted in terms of trajectory or standard band-structure effects and remains an open issue. At the present time, attempts to resolve this question are made difficult because there is no published calculation of the $SrRuO_3$ band structure, to our knowledge.

The strong signature of negative MR in the longitudinal geometry reveals that this component is *independent* of the Lorentz force, and hence is *not* an orbital effect. This in itself indicates some form of magnetic scattering. The observed negative MR is almost certainly due to the suppression of spin-flip scattering in a field, since this is commonly observed in ferromagnetic materials.[24] Recently, Klein *et al.*[25] investigated the magnetic and magneto-optic properties of $SrRuO_3$ thin films and reported that the temperature dependence of the magnetization is dominated by spin-wave excitations. Spin-flip or spin-exchange scattering between conduction electrons and such excitations could reasonably account for the negative MR behavior. This occurs, for example, in such itinerant ferromagnets as $ZrZn_2$ and Sc_3In,[26] where exchange-coupled scattering between nonmagnetic s-band carriers and collective fluctuations of itinerant magnetic d-band carriers dominates the low-temperature magneto-transport behavior. In fact, the field and temperature dependencies of the MR behavior in $SrRuO_3$ are strongly reminiscent of the behavior reported for these classic itinerant ferromagnets.

Hysteresis. There is clearly a large hysteresis effect in the MR and magnetization data. The thin-film coercive force and saturation field can be clearly identified both in the MR "butterfly" plot and in the M vs H hysteresis loop data (Fig. 4). The measured values for the coercive force (0.5–1 T) and the saturation field (3–4 T) in both measurements are very large compared to those for common ferromagnetic films. For example, typical values for NiFe films are on the order of tens of gauss. Most likely, the large fields indicate strong pinning in $SrRuO_3$ films. The pinning is not a truly intrinsic property of the material, but is strongly dependent upon the defect structure in each individual thin-film sample. The epitaxial growth process allows for grain boundaries to form, providing domain-wall pinning sites that normally would not be present in single crystals. This is illustrated by comparing our observed thin-film coercive force ($\sim$10 kG) to measurements on $SrRuO_3$ single crystals ($\sim$3 kG) reported in Ref. 2.

Phase transition. The second-order ferromagnetic phase transition itself is well represented by mean-field theory. The plot of $(d\rho/dT)$ in zero field shows a discontinuous jump at T_c. Such a jump is well known to be characteristic of the specific heat (c_v) through a second-order phase transition,[19] so that $d\rho/dT$ is proportional to c_v near T_c, as expected from standard theory.

We have shown through the field-cooled resistivity data that the kink in the zero-field resistivity near T_c is smoothed out in high magnetic fields. There are no anomalies through 160 K in the 5.2 T field-cooled $d\rho/dT$ data. Thus the field suppresses the ferromagnetic phase transition. The resistivity in a field from $\sim$70 to 200 K is always lower than the zero-field resistivity (i.e., negative MR). Because of the suppression of the resistivity kink at T_c by the magnetic field, the largest difference between the resistivity in field and zero field occurs near T_c. This suppression of the phase transition thus explains why the negative MR shown in Fig. 5 has a dip at T_c.

V. SUMMARY

The magnetoresistance characteristics of $SrRuO_3$ thin films have been measured from well below to just above the Curie point. At low temperatures, the magnetoresistance is determined by a competition between a positive orbital effect, which is Lorentz force dependent, and a negative spin-flip suppression, which is independent of the Lorentz force. The magnitude and functional form of the TMR data are not fully consistent with conventional trajectory or generic band-structure effects in the weak-field limit. The TMR and LMR behaviors are at least qualitatively similar to what is observed in itinerant ferromagnets. Hysteresis effects are observed with very large characteristic fields, indicating that there is unusually strong domain-wall pinning in these thin-film samples. One source of such pinning may be in the grain boundary structure in these films. The magnetic behavior through the Curie point is well represented by mean-field theory. The magnetoresistance shows that the phase transition is suppressed by an external magnetic field.

ACKNOWLEDGMENTS

We thank C. Gardner of Quantum Design for making a superconducting quantum interference device (SQUID) magnetometer available to us, and A. Dorsey and T. H. Geballe for enlightening discussions. C.B.E. acknowledges support from the NSF.

[1]G. L. Catchen, T. M. Rearick, and D. G. Schlom, Phys. Rev. B **49**, 318 (1994).

[2]J. J. Randall and R. Ward, J. Am. Chem. Soc. **81**, 2629 (1959).

[3]The orthorhombic (O) and perovskite (P) Miller indices are related by $[110]^O=[100]^P$, $[-110]^O=[010]^P$, and $[002]^O=[001]^P$.

[4]A. Callaghan, C. W. Moeller, and R. Ward, Inorg. Chem. **5**, 1572 (1966).

[5]J. M. Longo, P. M. Raccah, and J. B. Goodenough, J. Appl. Phys. **39**, 1327 (1968).
[6]A. Kanbayashi, J. Phys. Soc. Jpn. **41**, 1876 (1976); **44**, 108 (1978).
[7]C. W. Jones, P. D. Battle, P. Lightfoot, and W. T. A. Harrison, Acta Crystallogr. Sect. C **45**, 365 (1989).
[8]C. B. Eom, R. J. Cava, R. M. Fleming, J. M. Phillips, R. B. van Dover, J. H. Marshall, J. W. P. Hsu, J. J. Krajewski, and W. F. Peck, Science **258**, 1766 (1992).
[9]L. Antognazza, K. Char, T. H. Geballe, L. L. H. King, and A. W. Sleight, Appl. Phys. Lett. **63**, 1005 (1993).
[10]P. Tiwari, X. D. Wu, S. R. Foltyn, M. Q. Le, I. H. Campbell, R. C. Dye, and R. E. Meunchausen, Appl. Phys. Lett. **64**, 634 (1994).
[11]R. Domei, C. L. Jia, C. Copetti, G. Ockenfuss, and A. I. Braginski, Supercond. Sci. Technol. **7**, 277 (1994).
[12]A. A. Abrikosov, *Fundamentals of the Theory of Metals* (North-Holland, New York, 1988).
[13]J. M. Ziman, *Principles of the Theory of Solids* (Cambridge University Press, Cambridge, England, 1972), pp. 250–254.
[14]C. Herring, in *Magnetism,* edited by G. Rado and H. Suhl (Academic, New York, 1966), Vol. IV.
[15]D. L. Mills and P. Lederer, J. Phys. Chem. Solids **27**, 1805 (1966).
[16]T. Moriya, *Spin Fluctuations in Itinerant Electron Magnetism* (Springer-Verlag, New York, 1985).
[17]F. Reif, *Fundamentals of Statistical and Thermal Physics* (McGraw-Hill, New York, 1965).
[18]P. C. Hohenberg and B. I. Halperin, Rev. Mod. Phys. **49**, 435 (1977).
[19]S. K. Ma, *Modern Theory of Critical Phenomena* (Benjamin Cummings, Reading, MA, 1976).
[20]N. W. Ashcroft and N. D. Mermin, *Solid State Physics* (Sanders, New York, 1976).
[21]C. B. Eom, J. Z. Sun, K. Yamamoto, A. F. Marshall, K. E. Luther, T. H. Geballe, and S. S. Laderman, Appl. Phys. Lett. **55**, 595 (1989).
[22]C. B. Eom, J. Z. Sun, B. M. Lairson, S. K. Streiffer, A. F. Marshall, K. Yamamoto, S. M. Anlage, J. C. Bravman, S. S. Laderman, R. C. Taber, R. D. Jacowitz, and T. H. Geballe, Physica C **171**, 351 (1990).
[23]S. C. Gausepohl, Mark Lee, and K. Char (unpublished).
[24]E. P. Wohlfarth, in *Ferromagnetic Materials,* edited by E. P. Wohlfarth (North-Holland, Amsterdam, 1980), Vol. 1, Chap. 1; T. Moriya *ibid.*, Chap. 5, and references therein.
[25]L. Klein, J. S. Dodge, T. H. Geballe, A. Kapitulnik, A. F. Marshall, L. Antognazza, and K. Char, Appl. Phys. Lett. (to be published).
[26]S. Ogawa, Physica B&C **91**, 82 (1977); Y. Masuda, T. Hioki, and A. Oota, *ibid.* **91**, 291 (1977).